Journal of Biomolecular NMR, **22:** 107–122, 2002.
KLUWER/ESCOM

A quick solution structure determination of the fully oxidized double mutant K9-10A cytochrome c_7 from *Desulfuromonas acetoxidans* and mechanistic implications

Michael Assfalg[a], Ivano Bertini[a,*], Paola Turano[a], Mireille Bruschi[b], Marie-Claire Durand[b], Marie-Thérèse Giudici-Orticoni[b] & Alain Dolla[b]
[a]*Magnetic Resonance Center and Department of Chemistry, University of Florence, 50019 Sesto Fiorentino, Florence, Italy;* [b]*Unité de Bioénergétique et d'Ingénierie des Protéines, IBSM, Centre National de la Recherche Scientifique, 13402 Marseille Cedex, France*

Received 26 July 2001; Accepted 14 November 2001

Key words: automatic assignment, cytochrome c_7, electron transfer, multiheme cytochromes, NMR solution structure

Abstract

Lysines 9 and 10 in *Desulfuromonas acetoxidans* cytochrome c_7, which could be involved in the interaction mechanism with the redox partners, have been replaced by alanine residues using site-directed mutagenesis. The solution structure of the fully oxidized form of K9-10A cytochrome c_7, which is paramagnetic with three paramagnetic centers, has been determined via ^{1}H NMR. The assignment of the spectra has been performed through an automatic program whose algorithm and strategy are here described. The assignment of the NOESY spectra has been further extended by back calculating the NOESY maps. The final number of meaningful NOE-based upper distance limits was 1186. In the Restrained Energy Minimization calculations, 147 pseudocontact shift constraints were also included, which showed consistency with NOE-based constraints and therefore further contribute to validate the structure quality. A final family of 35 conformers was calculated with RMSD values with respect to the mean structure of 0.69 ± 0.17 Å and 1.05 ± 0.14 Å for the backbone and heavy atoms, respectively. The overall fold of the molecule is maintained with respect to the native protein. The loop present between heme III and heme IV results to be highly disordered also in the present structure although its overall shape mainly resembles that of the oxidized native protein, and the two strands which give rise to the short β-sheet present at the N-terminus and connected by a turn containing the mutated residues, are less clearly defined. If this loop is neglected, the RMSD values are 0.52 ± 0.07 Å and 0.92 ± 0.06 Å for the backbone and heavy atoms, respectively, which represent a reasonable resolution. The relative distances and orientations of the three hemes are maintained, as well as the orientation of the imidazole rings of the axial histidine ligands, with the only exception of heme IV. Such difference probably reflects minor conformational changes due to the substitution of the vicinal Lys10 with an Ala.
The replacement of the two lysines does not affect the reduction potentials of the three hemes, consistently with the expectations on the basis of the structure and electrostatic calculations. However, the replacement of the two lysines affects the reactivity of the mutant cytochrome c_7 with [Fe] hydrogenase, inducing a change in K_m. This finding is in agreement with the identification of the protein area around heme IV as the interacting site.

*To whom correspondence should be addressed. E-mail: bertini@cerm.unifi.it

Introduction

Multihemic c-type cytochromes, class III cytochromes according to Ambler (1991), are found in sulfate and sulfur reducing bacteria. The most studied of these cytochromes is the tetrahemic cytochrome c_3 present in the genus *Desulfovibrio*. Its three-dimensional structure known for several strains, shows a conserved spatial arrangement of the four hemes, despite the low sequence homology of the polypeptidic chain (Matias et al., 1996). A triheme cytochrome known as cytochrome $c_{551.5}$ or c_7 isolated from the sulfur reducing bacteria *Desulforomonas acetoxidans* (Probst et al., 1977), is a 68-aminoacid hemoprotein which retains the characteristic features of cytochrome c_3, i.e., bis histidine axial coordination and low redox potentials for the iron atoms (Moura et al., 1984). NMR studies of the iron(II) and iron(III) states (Coutinho et al., 1996; Turner et al., 1997; Banci et al., 1996; Assfalg et al., 1998, 1999) and the recently determined X-ray structure (Czjzek et al., 2001) have shown that cytochrome c_7 is structurally analogous to cytochrome c_3, with deletion of heme II (hemes are numbered according to the sequence order of the binding cysteinyl residues) and the corresponding peptidic attachment sequence. They establish the structural homology of the three hemes with hemes I, III and IV of cytochrome c_3. As in most cytochromes c_3, the high potential heme is the one analogous to heme IV (Morais et al., 1995). Electrostatic interactions in c_3 cytochromes between basic groups which surround heme IV crevice and acidic groups of the physiological partner hydrogenase have been demonstrated to be important for molecular recognition (Cambillau et al., 1988; Dolla et al., 1991).

The physiological partner of cyt c_7 has not been identified, although cyt c_7 has been shown to react with the recently identified and characterized [NiFe]hydrogenase from *D. acetoxidans* (Brugna et al., 1999). Cyt c_7 is also shown to react with the [Fe]hydrogenase from *Desulfovibrio* species.

In order to characterize the interacting site of cyt c_7, we have prepared a modified cytochrome in which two of the lysines surrounding the heme IV crevice, K9 and K10 are substituted by Ala residues. Reactivity of this mutant cytochrome with the [Fe]hydrogenase is described.

The solution structure of the mutant has been determined by NMR spectroscopy. In the frame of a project dealing with the development of new approaches that allow quick determination of solution structure of proteins, we have developed an automatic assignment program which relies on the availability of the assignment of an analogous protein of known structure. The expected NOESY patterns for the new protein can be recalculated on the basis of the structure of the old protein and the NOESY maps are reassigned by comparing the expected patterns and shifts with the actual ones. This procedure is expected to be particularly useful in the case of mutants. The approach resulted to be successful and allowed us to obtain the assignment and then the solution structure by analyzing only two NOESY maps of the protein.

Materials and methods

Bacterial strains and growth conditions

Strains and plasmids used in this study are described in Table 1. *Desulfovibrio desulfuricans* G201 was grown in milieu C (Postgate, 1984) supplemented with 0.28 mM kanamycin when required.

Site-directed mutagenesis

Replacement of K9 and K10 was achieved by site-directed mutagenesis. Oligonucleotide, K910A1, (5′-GTGACGTATGAGAATGCGGCGGGCAACGTTAC CTTT-3′) and its complement (K910A2), were designed in order to replace codons AAGAAG at nucleotides 203–208 in the *cyaA* sequence (Aubert et al., 1998) by GCGGCG encoding two alanine residues. The mutation was introduced in the gene by PCR as previously described (Ansaldi et al., 1996). Bacteriophage mpc3c7 (Aubert et al., 1998) was used as template in the PCR reaction. The mutation was checked by DNA sequencing. The mutated amplicon was then digested by both *Eco*RI and *Hin*dIII and subcloned in pBMK7 previously digested by the same enzymes to give pK7C7K910A.

This vector was further introduced into *D. desulfuricans* G201 by electrotransformation as previously described (Aubert et al., 1998). Recombinant *D. desulfuricans* G201 (pK7C7K910A) was selected on milieu C supplemented with 0.28 mM Kanamycin and the presence of the vector was checked by Plasmid DNA mini-preparation as described in Maniatis et al. (1989) (Sambrook et al., 1989).

Table 1. Bacterial strains and vectors used

Desulfovibrio desulfuricans G201	Spontaneous Nal^r derivative of *D. desulfuricans* G100A (Weimar et al., 1988)
mpc3c7	A derivative of mp18cycHS that contains *cyc-cyaA* gene fusion (Aubert et al., 1998)
pBMK7	Broad-host range vector, Km^r (Rousset et al., 1998)
pK7C7K910A	Contains *cyc-cyaA* gene fusion carrying the mutations on a 530-bp *Eco*RI-*Hin*dIII insert in pBMK7 (this study)

K9-10A cytochrome c_7 purification and characterization

Recombinant *D. desulfuricans* G201 (pK7C7K910A) cells (265 g, wet weight) were obtained from 300 l culture of medium C. Cells were harvested, resuspended in 300 ml of 100 mM Tris-HCl-100 mM EDTA (pH 9) buffer, and stirred for 30 min at 37 °C in a water bath. The mixture was then centrifuged at 27 000 × *g* for 1 h at 4 °C, and the resulting supernatant was dialyzed overnight against distilled water at 4 °C. This periplasmic extract was loaded onto a column of DEAE-cellulose (Whatman DE 52) equilibrated with 10 mM Tris-HCl, pH 7.6. The unadsorbed fraction that contained cytochrome c_7 was then applied to a hydroxyapatite (Bio-Rad) column equilibrated with 10 mM Tris-HCl (pH 7.6). The cytochrome c_7-containing fraction was eluted with 300 mM phosphate buffer (pH 7.6) and concentrated by ultrafiltration on a Centriprep Centrifugal Filter Device YM-3 (Amicon). This concentrated fraction was then loaded onto a Superdex 75 column equilibrated with 50 mM Tris-HCl-100 mM NaCl buffer (pH 7.6). K9-10A cytochrome c_7 was found to be pure after this last step. The purity of the samples was analyzed by polyacrylamide gel electrophoresis under denaturing conditions (PhastSystem; Pharmacia) and by N-terminal sequence determination (Applied Biosystems A470 Gas Phase Sequenator). Amino acid analyses were carried out on a Beckman amino acid analyzer (system 6300). The reduction potentials were determined by electrochemistry as previously described (Haladjian et al., 1994).

The molecular mass of both wild-type and K9-10A cytochromes c_7 were determined on a reflextran time of flight mass spectrometer equipped with delayed extraction (Voyager DE-RP, Perceptive Biosystems Inc.). 0.7 µl of sample was directly mixed on the support with an equal volume of matrix (saturated solution of sinapinic acid in 40% acetonitrile, 60% water made 0.1% in trifluoracetic acid).

Kinetics of electron transfer

Reduction by [Fe] hydrogenase from *D. vulgaris* Hildenborough was achieved using anaerobic cuvettes, filled with 50 mM HEPES (pH 7), 25 mM glucose, 0.5 U ml^{-1} glucose oxidase and 250 U ml^{-1} catalase as previously described (Aubert et al., 1998) and various concentrations of either wild-type or K9-10A cytochromes c_7. The cytochrome reduction rate at room temperature was determined from the absorption band at 553 nm and by using the slope of the tangent drawn at the beginning of the recording.

NMR spectroscopy

The ^{1}H-NMR samples was prepared by dissolving the lyophilized protein in 100 mM phosphate buffer, pH 6.5, to give 2–3 mM solutions.

The ^{1}H-NMR spectra were recorded on a Bruker AVANCE 800 spectrometer operating at 800.13 MHz. A time proportional phase increment (TPPI) NOESY (Macura et al., 1982; Marion and Wüthrich, 1983) spectrum was recorded at 298 K in H_2O solution on a spectral width of 50 ppm with a recycle time of 275 ms and a mixing time of 100 ms. This spectrum was obtained by presaturating the residual water resonance during the relaxation delay and the mixing time. To optimize the observation of connectivities in the diamagnetic region, another TPPI NOESY map in H_2O solution at 298 K was recorded on a smaller spectral width (22 ppm) with a recycle time of 658 ms, a mixing time of 100 ms and water suppres-

sion by gradient-tailored excitation (WATERGATE) (Piotto et al., 1992).

Both two-dimensional spectra consisted of 2 K data points in the F2 dimension. 1024 experiments were recorded in the F1 dimension, using 80 and 256 scans for the spectrum with smaller and larger spectral width, respectively. Raw data were multiplied in both dimensions by a pure cosine-squared bell window function and Fourier-transformed to obtain 1024x1024 real data points. A polynomial base-line correction was applied in both directions.

Data processing was performed using the standard Bruker software package. The 2D maps were analyzed with the aid of the program XEASY (Bartels et al., 1995).

Assignment strategy

The assignment of the protein resonances was performed through a procedure which consists of the prediction of the NOE connectivities and the subsequent automatic assignment of the experimental NOESY cross-peaks. Expected NOE connectivities were calculated with the CORMA program (Borgias et al., 1989), which is based on a relaxation matrix approach, considering the experimental mixing time. For this purpose, a structural model has been generated through the MOLMOL program (Koradi et al., 1996) by simply introducing the two mutations in the energy minimized average structure of the native protein. The proton chemical shifts of the native protein was used to generate the expected NOESY peak list. The NOESY map recorded on the diamagnetic spectral width was used as the spectrum for the automatic assignment. The peaks have been picked by the automatic peak-picking routine of the XEASY program (Bartels et al., 1995). The peak list was assigned with the use of a new-developed software program (Homology-based Assignment of Noesy Spectra; HANS, available at the site www.postgenomicnmr.net). This program compares the NOEs networks of the reference native protein with those of the mutant. The input files are the assigned NOESY peak list of the reference system and the unassigned peak list of the system to be determined. For each expected peak, candidate peaks are selected within a certain distance in terms of chemical shift. The combinations of candidate peaks give rise to candidate frequencies, which can be assigned on the basis of the given NOE patterns and the alignment of peaks corresponding to the same frequency. Resonances and NOEs are assigned when an acceptable number of expected peaks within a pattern can be retrieved on the new spectrum. A relaxation matrix approach based on the CORMA program has been used to complete the assignment of the NOESY maps, as described in the Results section.

Proton-proton distance constraints

The volumes of the NOESY cross peaks between assigned resonances were obtained by manual integration, with the elliptical integration routine implemented in the program XEASY (Bartels et al., 1995). NOESY cross peak intensities were converted into upper limits of interatomic distances by following the methodology of the program CALIBA (Güntert et al., 1991).

Pseudocontact-shift constraints

Pseudocontact shifts arise from the magnetic susceptibility anisotropy and depend on the nuclear position with respect to the principal axes of the magnetic susceptibility tensor (Bertini and Luchinat, 1986, 1996). Therefore they contain structural information and can be used as structural constraints, once the magnetic anisotropy tensor parameters are given (Banci et al., 1996, 1997, 1998). They are long range constraints, as they decrease with the reciprocal of the third power of the metal-nucleus distance. In this work they were used during the energy minimization procedure, as already reported for the fully oxidized native protein. Apparently, three close paramagnetic centers all contributing to the pseudocontact shifts of most protons prevent the use of pseudocontact shift constraints from random structures and can only be used for structural refinement.

The pseudocontact shift values were obtained by subtracting the chemical shifts measured for the totally reduced, diamagnetic form of the native protein, from the corresponding shifts of the completely oxidized, paramagnetic form. This choice of the diamagnetic reference is justified by the essential identity between the structures of the native and mutated protein, as it results from preliminary calculations based on distance constraints only. The total number of pseudocontact shifts used for evaluating the magnetic susceptibility tensor and structural refinement was 147.

Experimentally determined pseudocontact shift values were used for the determination of the magnetic anisotropy tensor parameters. The fifteen independent magnetic susceptibility anisotropy tensor parameters

(five parameters are needed to describe each tensor: $\Delta\chi_{ax}$, $\Delta\chi_{rh}$, and three independent direction cosines that define the principal directions of the χ tensor with respect to the chosen axis system) could be evaluated using the position vectors for each proton obtained for each structure of the starting family and the set of experimental pseudocontact shift values. The calculation was performed with the program FANTASIAN (Banci et al., 1996, 1997), as already reported for the native cytochrome c_7 and other proteins. A preliminary set of magnetic anisotropy tensor parameters was obtained by running the program FANTASIAN over the family of structures determined by DYANA (see below). These values were used as input for the minimization procedure. Another set of magnetic susceptibility tensor parameters was calculated over the family of minimized structures and used for obtaining information about the electronic structure of the paramagnetic centers. Errors were estimated with a Montecarlo approach by performing 200 different calculations where 30% of structures and 30% of shift values were randomly eliminated from input data.

Structure calculations

The experimental distance constraints were used to generate protein conformers using the DYANA program (Güntert et al., 1997). A residue containing the heme moiety was added to the standard library as a protein residue, as previously reported (Banci et al., 1995, 1996, 1997). Also the links between the iron atoms and their axial ligands and between the heme and the heme-bound cysteine residues have been introduced in analogy to previous papers

1514 distance constraints derived from 2D NOESY connectivities were used in DYANA calculations. 25 stereo specific assignments were obtained through the program GLOMSA (Güntert et al., 1991). 500 random structures were annealed in 10 000 steps using the above constraints. The 35 structures with the lowest target function were included in the family.

Restrained energy minimization (REM) with the Sander module of Amber was applied to the 35 structures of the DYANA family (Pearlman and Case, 1991; Case et al., 1999). A REM calculation was performed by applying the NOE constraints only. A further REM calculation was performed introducing both NOE and pseudocontact shift constraints. Pseudocontact shifts were included as constraints through a modified Sander module (PSEUDOREM) (Banci et al., 1997), as already reported for the fully oxidized native protein. The magnetic anisotropy parameters needed for this calculation were obtained by running the program FANTASIAN (Banci et al., 1996, 1997) over the family of structures calculated with DYANA.

Structure analysis

The quality of the final family of structures has been analyzed in terms of ideal geometry parameters with the Procheck-NMR program (Laskowski et al., 1996).

Electrostatic potential calculations

The present energy minimized averaged solution structure was used as starting data. The structure was solvated with a 100 nm thick shell of water molecules. The water molecules were equilibrated through energy minimization and molecular dynamics calculations, keeping the protein atoms fixed. Finally the whole system (water + protein) was energy minimized. The electrostatic potential calculations were performed with the DelPhi program package (Gilson et al., 1985; Klapper et al., 1986; Gunner and Honig, 1991) using the same protocol and parameters as for the native protein (Assfalg et al., 1999).

Results and discussion

K9-10A cytochrome c_7 purification and characterization

Expression of the gene encoding K9-10A cytochrome c_7 into *D. desulfuricans* G201 led to the purification of 22 mg of cytochrome from 265 g of cells. The yield of production is similar to that obtained when wild-type cytochrome c_7 was produced in the same organism (Aubert et al., 1998) suggesting that replacement of the two K residues has no effect on the production of the protein. The N-terminal sequence of K9-10A cytochrome c_7 is similar as that of wild-type protein except at positions 9 and 10 where lysine residues are replaced by alanines. The molecular mass determined by mass spectrometry is in agreement with lysine replacements by alanine and with the binding of three hemes per molecule (MW mutant = 8993.96, MW native = 9108.93).

^{1}H NMR spectra

The 1D NMR spectrum of the fully oxidized K9-10A mutant of cytochrome c_7 is reported in Figure 1, where

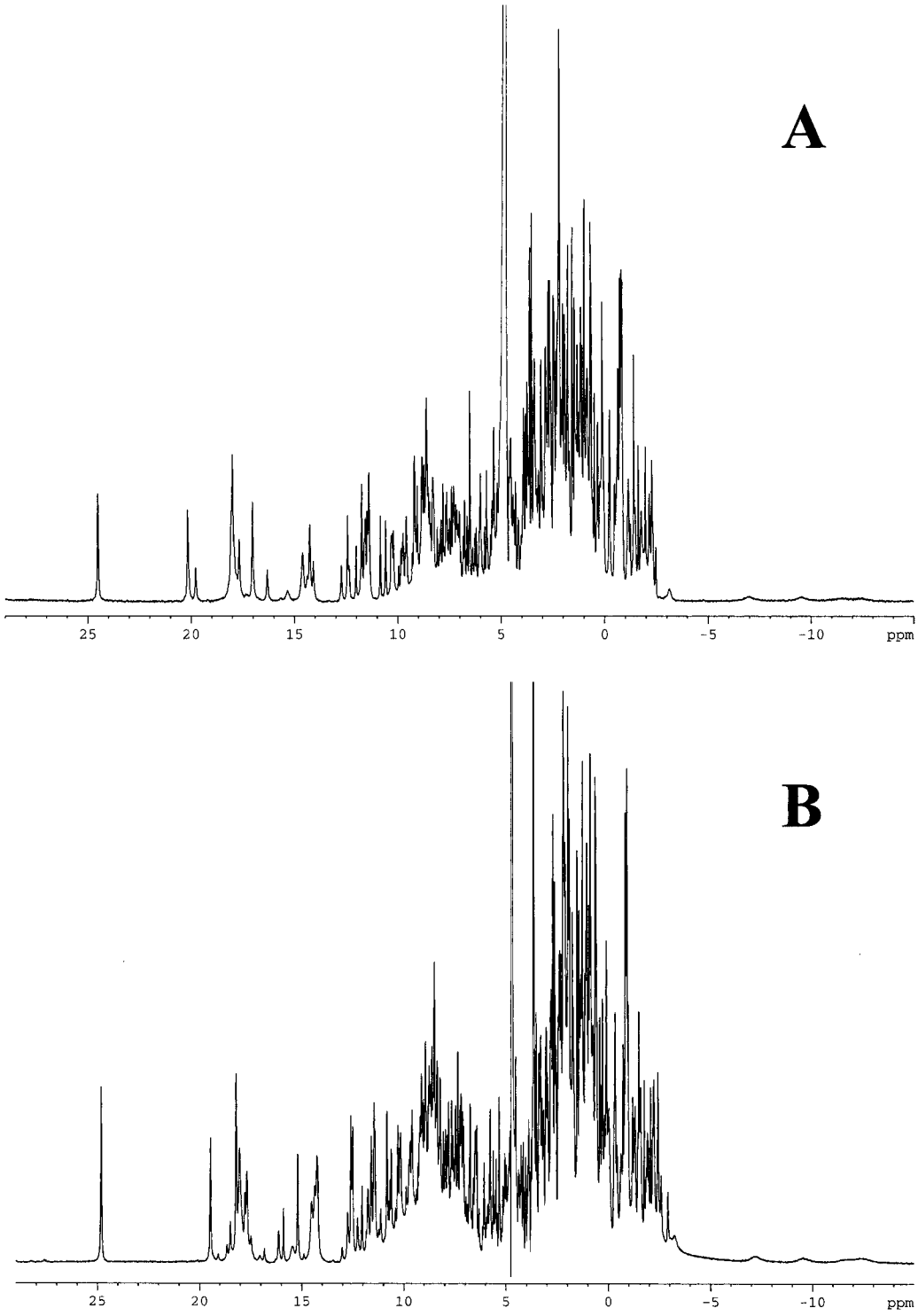

Figure 1. 800 MHz ^{1}H NMR spectra of the fully oxidized native (A) and K9-10A cytochrome c_7 (B) recorded in 100 mM phosphate buffer, pH 6.5 and 298 K.

Table 2. Heme methyl shifts for the fully oxidized K9A K10A and wild type cytochrome c_7. The shift values are measured in H_2O solution with 100 mM phosphate buffer, pH 6.5 and 298 K

Heme	Methyl	K9A K10A	WT
I	1-CH_3	8.63	8.63
I	3-CH_3	18.31	18.00
I	5-CH_3	9.08	9.23
I	8-CH_3	24.91	24.53
III	1-CH_3	14.63	14.63
III	3-CH_3	14.38	14.28
III	5-CH_3	18.12	18.04
III	8-CH_3	−0.84	−0.77
IV	1-CH_3	15.31	17.03
IV	3-CH_3	9.27	8.84
IV	5-CH_3	19.56	20.17
IV	8-CH_3	12.71	11.76

it is compared with the corresponding spectrum of the fully oxidized native protein. The spectra are very similar besides minor differences in chemical shifts for some of the heme resonances (Table 2). Moreover, resonances attributable to a minor species could also be detected. The presence of a minor species can also be inferred by the analysis of the 2D NOESY maps. Some NOESY patterns are clearly doubled, the separation between the corresponding resonances never exceeding 0.75 ppm. In other cases the presence of a minor species can be inferred by small shoulders of the main peaks. The ratio between the major form (hereafter called form A) and the minor one (form B, hereafter) is about 3:1. As N-terminal sequence, amino acid composition and mass spectrometry showed that the protein is pure with respect to the sensibility of these methods, the presence of two species could reasonably be attributed to the presence of two conformers in slow exchange on the NMR time scale. By analyzing the distribution of residues clearly giving rise to splitting effects (i.e., residues 4–6, 8–15, 18–20, 37–54, 63–66, and selected heme resonances) in the NMR spectra we can interpret the presence of the minor species in terms of two possible conformations of the loop containing the two mutated residues. This would reflect also on the conformation of the two β-strands connected by this loop, on the straight polypeptide fragment facing the β-sheet and some of the residues spatially close to these structural elements.

NMR spectra assignment

The automatic peak picking of the diamagnetic NOESY map resulted in 2200 peaks, including those of the minor species. A quite high contour level was chosen in order to avoid picking of noise. Evident artifact peaks were removed and further peaks or shoulders were picked manually. The final peak list, constituted by about 2400 peaks, was used for the automatic assignment procedure.

3300 NOE connectivities were back calculated through the CORMA program using a model structure for K9-10A cyt c_7, as described in Materials and methods, and the proton chemical shifts of the native oxidized protein. For simplicity, the effect of paramagnetism on proton relaxation was not introduced in this relaxation matrix approach. This implies that some of the calculated connectivities may not be observable in practice. A 100 ms mixing time and a 4 ns correlation time for the tumbling of the molecule were used as input parameters. The output peak list was obtained by introducing a value of 0.01 for the cutoff level of the intensities. The latter peak list and the one corresponding to the experimental NOESY map, were used as input for the automatic assignment program HANS.

Cross-peaks connecting unassigned resonances were identified from the NOESY patterns expected on the basis of the CORMA output. A final number of 2394 and 353 peaks were assigned in the diamagnetic and paramagnetic NOESY map, respectively.

At the end, a total number of 367 proton resonances were assigned, which correspond to 77.4% of the total expected proton signals (75.6% of the amino acid residues, 88.3% of the heme resonances). The backbone protons for all residues except Ala1 were identified.

The use of the HANS program resulted precious for a quick assignment of the present system, being available the NMR assignment of the native protein. Although the analysis was complicated by the presence of two species, HANS program provided 632 out of 2400 peaks, which correspond to 174 protein resonances and 43 residues assigned. From interactive analysis at this stage and *a posteriori* checking through back-calculation, 96% of the resonances were found to be correctly assigned.

The present paper reports the first example of the application of this new protocol for the quick obtainment of structural data of proteins, using an assignment strategy based on the similarity of chemical shifts and reproducibility of NOESY patterns between

the system under investigation and a reference system. At variance with other more sophisticated programs for automatic assignment of NMR spectra, the HANS program has an applicability limited to the analysis of NMR spectra of mutants or proteins with high homology to a reference protein whose NMR assignment is already available and for which a structural model exists. However, it represents a simple and useful tool in the NMR scenario.

Solution structure calculations

1514 unique NOESY experimental constraints were obtained, and their distribution is shown in Figure 2A. These NOE constraints were transformed into upper distance limits with the program CALIBA (Güntert et al., 1991), which uses a volume-to-distance correlation. The best calibration of observed intensities was found to be inversely proportional to the fourth, fifth or sixth power of the proton-proton distances, depending on the calibration class of NOE constraints.

1186 out of the total 1514 experimental constraints were found to be meaningful and therefore used in the DYANA calculations. The average number of experimental and meaningful NOE constraints per residue is 21.3 and 16.7, respectively (considering each heme as a further protein residue). The resulting family, constituted by 35 conformers, experiences target function values in the 0.36–0.57 $Å^2$ range, resulting in a mean value of 0.49 ± 0.06 $Å^2$. The conformers have RMSD values to the mean structure of 0.70 ± 0.16 Å and 1.10 ± 0.15 Å for the backbone and heavy atoms, respectively.

Each conformer of the family was subjected to REM calculations. The RMSD and target function values for the resulting family (Figure 3) are reported in Table 3. The protein regions characterized by the largest RMSD values in Figure 2B correspond to those containing not-assigned residues and/or residues for which a limited number of NOESY connectivities could be assigned (Figure 2A). In particular, the loop involving residues 56–61 results quite disordered. RMSD values calculated superimposing residues 3-55 and 62-66 are significantly lower: 0.52 ± 0.07 Å and 0.92 ± 0.06 Å for the backbone and heavy atoms, respectively. A similar feature was also found for the native protein (Assfalg et al., 1998; Assfalg et al., 1999) and probably reflects an intrinsic disorder of this external loop.

An analogous REM calculation was performed on the conformers obtained from DYANA using as experimental constraints both the NOE-derived upper distance limits and the pseudocontact shifts, as described in the Experimental part. Although the introduction of pseudocontact shift-based constraints does not improve the precision of the family of conformers, the consistency of the two sets of experimental constraints contributes in further validating the quality of the assignment and of the resulting solution structure. Indeed, the structure obtained upon introduction of pseudocontact shift constraints is slightly different from that obtained with NOEs only, as revealed by the slightly different magnetic susceptibility tensor parameters.

The coordinates of the conformers of these final families were averaged and then energy-minimized.

Structure analysis

The accuracy of the calculated energy-minimized average structure was assessed by comparing the NOE connectivities calculated by the program CORMA (Borgias et al., 1989) with the experimental peaks. Paramagnetic effects were neglected. In particular we checked that all the cross peaks used in structural calculations corresponded to an expected peak and all the expected cross peaks (above a certain intensity threshold, which correspond to a proton-proton distance of about 4 Å) were identified in our spectrum. Moreover, we verified that all the well resolved peaks above a reasonable contour level in the 2D NOESY maps, corresponding to the assigned resonances of form A, were assigned, integrated, and used in the structure calculations. The fact that the two sets of different experimental constraints, i.e., NOE-based upper distance limits and pseudocontact shifts, are consistent with each other constitutes an additional proof of the accuracy of the obtained structure.

The parameters quantifying the agreement between the constraints and the final REM and PSEUDOREM families of structures, as well as the total energy, are summarized in Table 3. These figures are comparable with those found for the fully oxidized and fully reduced proteins (Assfalg et al., 1998, 1999). It is worthy to mention that the stereochemical PROCHECK analysis performed on the crystal structure gives a relatively low percentage of residues in the most favoured regions of the Ramachandran plot for 1.9 Å resolution.

The solution structure of the K9-10A shows an overall fold close to that of the fully oxidized and fully reduced native protein. The RMSD values between the

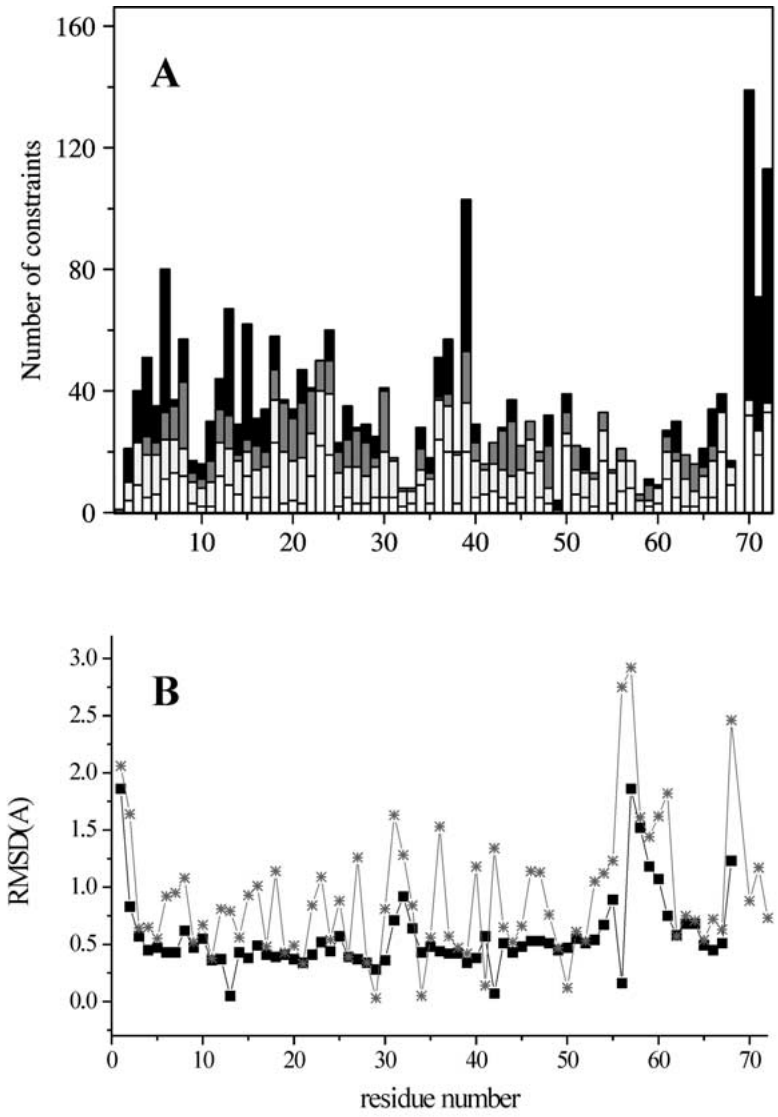

Figure 2. The number of observed experimental NOEs per residue (A) is compared with the RMSD per residue with respect to the average structure for the backbone (■) and all heavy atoms (∗) obtained for the restrained energy minimized family (B). Black bars in (A) indicate long range NOEs, dark grey medium range NOEs, light grey sequential NOEs, and white intraresidue NOEs. Residues 70, 71, 72 represent hemes I, III, and IV, respectively.

average structures of the oxidized mutant and oxidized native protein are 1.45 Å for the backbone and 1.73 Å for all the heavy atoms. The corresponding values, when the oxidized mutant and the reduced native are compared, are 1.44 and 1.81 Å. A β-sheet is composed by the 3–4 and 15–16 strands. Five helical segments are present at positions 17–24, 27–29, 43–46, 50–55 and 62–65. Therefore, as already observed in all the available structures of three- and tetraheme cytochromes from sulfur- and sulfate reducing bacteria, an *N*-terminus β-sheet, an α-helix containing the two distal ligands of heme I and III (His17 and His20 in cytochrome c_7), an α-helix preceding the proximal ligand of heme I (His30), an α-helix containing the distal ligand of heme IV (His45), an α-helix formed by the protein fragment around the proximal ligand of heme III (His53), and a C-terminal α-helix, are present. In the present structure the five helical fragments appear better defined than in the previous solution structures of cytochrome c_7. On the contrary, the *N*-terminal β-

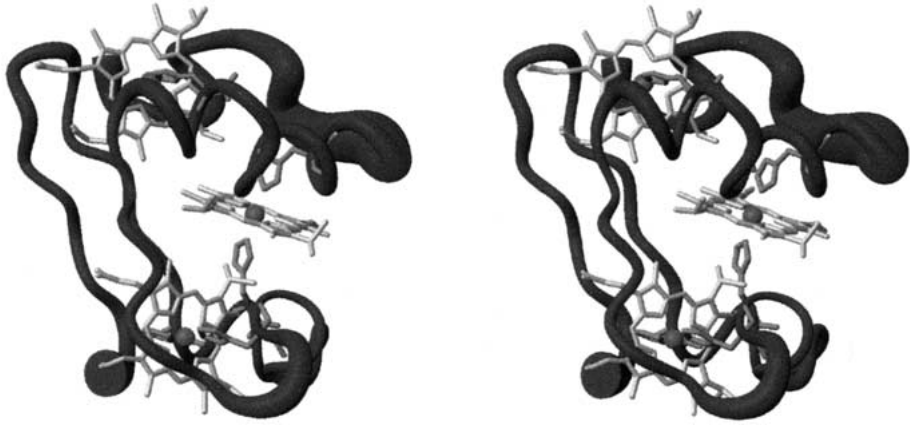

Figure 3. Stereoview of the backbone of the family of 35 structures calculated by restrained energy minimization shown as a tube with variable radius. The radius is proportional to the RMSD of each residue. The figure is generated with the MOLMOL program (Koradi et al., 1996).

sheet is less defined. As this sheet is formed by two strands connected by a turn containing the two mutated residues, it could be that the mutation induces a destabilization of this structural element.

Very recently, an X-ray crystal structure of native cytochrome c_7 became also available. As shown in Figure 4, the backbone fold is essentially superimposable with that of the present structure. The average RMSD values between the energy-minimized solution structure of K9-10A cytochrome c_7 and the crystal structure of the native protein are 1.17 Å and 1.72 Å for the backbone and heavy atoms, respectively, and the distribution of RMSD per residue is reported in Figure 5. The largest differences are observed for the protein fragments that correspond to the areas experiencing the larger RMSD values within the family of NMR solution structures. Interestingly, the same residues in the crystal structure are characterized by large B-factor values.

Parameters previously reported to evaluate the relative position of the three redox centers are the iron-iron distances, the angles between heme planes, and the angles between iron atoms. The values found in the present average energy minimized structure are reported in Table 4, where they are compared with those of the previously determined structures of cytochrome c_7, while a superimposition of the heme planes for the solution structure of mutant and the crystal structure of the native protein is reported in Figure 4B.

The differences in iron pair distances measured in the various structures are all within 1 Å. The angles between heme planes never differ by more than 26°, while the differences in the angles between iron atoms never exceed 8° along the series of structures. The observed variability in these parameters seems to be related to the indeterminacy of the structure, whereas none of these values seems to be specifically affected by the mutation at positions 9 and 10.

More attention should be devoted to the comparison of the axial histidine ligands. As already mentioned in the papers from our group (Assfalg et al., 1998, 1999), the conformation of the imidazole rings in the solution structures results from the few NOE constraints observed for some of these residues (and not the same in the various protein forms) and from steric requirements imposed by the protein fold. More significant are the conformational parameters obtained from the analysis of the heme methyls chemical shifts in the fully oxidized form, that allow to obtain information on the relative orientation of the imidazole planes of the two axial histidines and of the orientation of the bisector of the angle among them and the heme plane. In any case, in Figure 4C a comparison of the orientation of the His planes in the mutant and in the crystal structure is shown.

The information based on the heme methyls chemical shift is by far more sensitive than the accuracy of the structural data based on upper distance limits. For the present protein, small shift differences are found for the heme methyls with respect to the fully oxidized wild type protein (Table 2). The conformational data resulting from the analysis of these shift values are the following: (i) for heme I the angle between the two imidazole planes results 62.0° and the angle between the bisector and the plane perpendicular to the heme containing the N_A-Fe-N_C atoms results −103.2°; (ii) for heme III the corresponding angles are 19.8° and −28.9°, respectively; (iii) for heme IV the angles are

Table 3. Restraint violations and structural and energetic statistics for the solution structure of the fully oxidized K9A K10A cytochrome c_7.

	REM family	PSEUDOREM family
RMS violations per constraint (Å)		
Intra-residue (232)	0.020 ± 0.003	0.021 ± 0.004
Sequential (349)	0.016 ± 0.003	0.024 ± 0.006
Short range[a] (259)	0.010 ± 0.004	0.023 ± 0.012
Long range (475)	0.013 ± 0.002	0.022 ± 0.010
Total (1315)	0.015 ± 0.002	0.023 ± 0.007
Average number of violations per structure		
Intra-residue	7.4 ± 1.58	8.17 ± 1.61
Sequential	8.94 ± 2.66	11.25 ± 2.36
Short range[a]	3.60 ± 1.82	7.74 ± 2.06
Long range	6.71 ± 1.72	9.63 ± 2.50
Total	26.66 ± 4.21	36.8 ± 4.59
Average target function (Å^2)	0.32 ± 0.06	0.71 ± 0.36
Average no. of violations larger than 0.3 Å	0.06 ± 0.23	0.82 ± 1.25
Average no. of violations between 0.1-0.3 Å	7.45 ± 2.35[b]	15.8 ± 3.11[c]
Pseudocontact shift average target function (Å^2)	–	5.46 ± 1.54
Largest pseudocontact shift violation (ppm)	–	2.44[d]
AMBER force field average total energy (kJ mol^{-1})[e]	−4939.79 ± 223.76	−1690.55 ± 863.80
Structure precision (Å)[f]		
Backbone	0.69 ± 0.16	0.69 ± 0.17
All heavy atoms	1.09 ± 0.13	1.05 ± 0.14
Structural analysis[g]		
% of residues in disallowed regions	3.4[h]	3.4[h]
% of residues in generously allowed regions	1.7	3.4
% of residues in allowed regions	32.8	31.0
% of residues in most favorable regions	62.1	62.1

[a] Short range distance constraints are those between residues (i,i+2), (i,i+3), (i,i+4) and (i,i+5).
[b] The largest violation occurs in structure no. 25 for Hα/Hδ3 54 (0.309 Å).
[c] The largest violation occurs in structure no. 30 for 1-γCH_3 5-Hβ3 12 (1.34 Å).
[d] The largest violation occurs in structure no. 31 for the Hβ of Val 13.
[e] Excluding the NOE and pseudocontact shift constraints.
[f] The precision of the atomic coordinates is defined as the average RMSD between the 35 structures of the family and the mean coordinates.
[g] The reported values are referred to the energy minimized average structures.
[h] This value accounts for residues Cys26 and Cys49.

74.6° and 30.8°. The corresponding values for the native, fully oxidized protein were: 63.0° and −103.2° for heme I, 19.6° and −28.9° for heme III, 73.3° and 24.2° for heme IV. Therefore, the only meaningful, although relatively small, difference exists for heme IV. It is noteworthy to mention that this heme is the closest one to the mutation site and in particular that one of its axial ligands, His66, is spatially close to position 10. It could therefore be that the substitution of a positively charged long-chain residue as Lys10 with an alanine somehow affects the conformation of the imidazole ring of His66.

Small differences in the electronic properties of heme IV between the native and the mutated protein are also pointed out by the analysis of the magnetic susceptibility tensor parameters. The final magnetic susceptibility tensor, calculated over the 35 structures of the PSEUDOREM family, has $\Delta\chi_{ax} = (3.50 \pm 0.31) \times 10^{-32}$ m^3 and $\Delta\chi_{rh} = (-0.71 \pm 0.46) \times 10^{-32}$ m^3 for heme I, $\Delta\chi_{ax} = (3.42 \pm 0.35) \times 10^{-32}$ m^3 and $\Delta\chi_{rh} = (-0.71 \pm 0.47) \times 10^{-32}$ m^3 for heme III, and $\Delta\chi_{ax} = (3.36 \pm 0.31) \times 10^{-32}$ m^3 and $\Delta\chi_{rh} = (-0.90 \pm 0.40) \times 10^{-32}$ m^3 for heme IV. The x axis deviates about 5 ± 15° from the N_A-Fe-N_C direction in heme I, 54 ± 20°in heme III,

Table 4. Heme packing geometry and relevant conformational parameters defining the orientation of the axial histidine ligands for the energy minimized NMR solution structure of the K9-10A mutant with the X-ray crystal structure and NMR solution structures of the native protein. The figures reported in this Table for the native protein have been measured from the structure deposited in the PDB (PDB code 1hh5) and have been determined with the same method used for the previously published data for the solution structures of the fully reduced and fully oxidized native proteins. (The resulting numbers for the X-ray crystal structure are in some cases different from those reported in (Czjzek et al., 2001).)

	K9-10A cyt c7 NMR	Native cyt c_7 X-ray	Native cyt c_7 fully oxidized NMR	Native cyt c7 fully reduced NMR
Fe-Fe distances (Å)				
I–III	12.2	11.5	12.0	11.9
I–IV	18.6	19.3	18.3	18.9
III–IV	12.4	12.6	11.8	12.5
Angles among Fe atoms (°)				
I–III–IV	98.7	106	100.3	101.2
III–IV–I	40.2	35	40.2	38.2
III–I–IV	41.2	39	39.4	40.6
Angles between heme planes (°)				
I–III	45	28	31	41
I–IV	27	6	1	11
III–IV	60	52	68	56
Angles between His planes (°)[a]				
17–30 (I)	62	72.8	63	–
20–53 (III)	20	31.4	20	–
45–66 (IV)	75	101.2	73	–

[a]In the case of the solution NMR structure these values are derived from the heme methyl chemical shifts in the fully oxidized proteins.

and 77 ± 14° in heme IV. The deviation of the *z* axis from the perpendicular to the heme plane is 6 ± 5°, 5 ± 8°, 11 ± 5° for heme I, heme III, and heme IV, respectively. These values match those of the native protein, if allowance is made for the experimental error. The only exception is represented by the rhombic axes of heme IV, whose orientation results to differ by 20° from that of the native protein. The angle defining the orientation of the *x* component of the magnetic susceptibility tensor and the angle between the bisector to the angle between the two imidazole planes and the N_A-Fe-N_C direction, are theoretically predicted to be opposite in sign but equal in absolute value. This is the case for the present system, within the experimental error.

Heme redox potentials

The redox potentials for the three hemes in the mutated protein are −115 ± 10 mV, −165 ± 10 mV, −215 ± 10 mV. No differences are found, within the experimental error, with those of the native protein (−120 ± 10 mV, −172 ± 10 mV, −225 ± 10 mV, Aubert et al., 1998). This finding is in agreement with electrostatic calculations performed with the Delphi program (Gilson et al., 1985; Klapper et al., 1986; Gunner and Honig, 1991) over the present structure of the mutant. These calculations show that the relative reduction potentials are approximately the same as for the native protein. A slight increase in the reduction potential of heme IV is observed, but it is very small and it could be within the indetermination of the method. We conclude that the nature of the residues in positions 9 and 10 has an almost negligible effect on the reduction potential of iron IV in the wild type protein. These residues are probably too far from the heme moiety in terms of electrostatic interactions, and are not able to significantly affect the solvent accessibility to the heme.

Indeed, as reported in Figure 5, no meaningful differences are detected in solvent accessibility of the various residues in the mutant with respect to the native protein. Only slight increase (about 4%) in solvent accessibility is found for heme IV, as an effect of the substitution of the two long side chains of Lys9 and

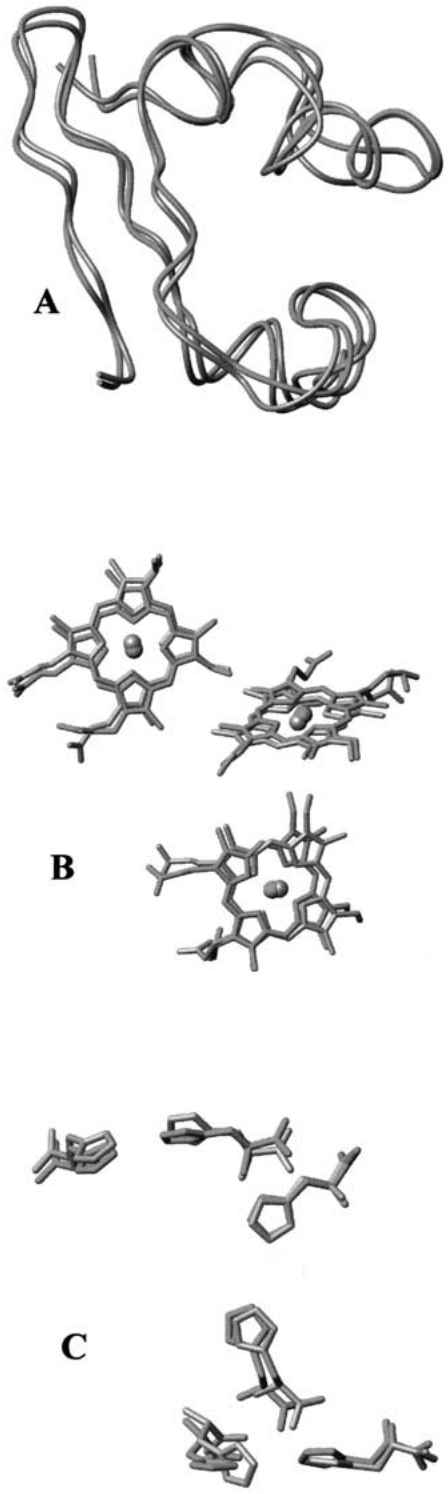

Figure 4. The energy minimized NMR solution structure of the K9-10A mutant (represented in red) is compared with the X-ray crystal structure of the native protein (represented in grey) in terms of backbone fold (A), heme orientations (B), and iron axial ligand conformations (C). The figure is generated with the MOLMOL program (Koradi et al., 1996).

10, that in the native structure are facing the heme propionates, with the short alanine residues.

Electron transfer with hydrogenases

Previous works have shown that cytochrome c_7 is reduced by either *D. acetoxidans* hydrogenase (Brugna et al., 1999) or *Desulfovibrio vulgaris* Hildenborough [Fe]hydrogenase (Assfalg et al., 1999). In order to analyze the effects of the mutations on the electron transfer properties of the cytochrome, the kinetics of reduction of both the wild-type and the mutant cytochromes by [Fe]hydrogenase from *D. vulgaris* Hildenborough, were studied. The steady state rate of reduction of both cytochromes followed Michaelis-Menten kinetics. The kinetic parameters are $k_{cat} = 35.1 \pm 6\ s^{-1}$ and $K_m = 35.2 \pm 12\ \mu M$ for the native protein, and $k_{cat} = 39.2 \pm 9\ s^{-1}$ and $K_m = 53.6 \pm 12\ \mu M$ for the mutant. While the catalytic constants are of the same order of magnitude, the K_m value is higher in the case of K9-10A cytochrome c_7 than in the case of wild-type cytochrome. This result suggests that the mutation affects the interaction between cytochrome and hydrogenase but has no effect on the electron transfer reaction.

Replacement of two lysines by alanine residues changes the charge around heme IV and thus should modify the interaction parameters with the redox partners. The kinetic data presented here are in agreement with this hypothesis and with the identification of heme IV as the interacting site for hydrogenase, as it is the case for cytochrome c_3 (Mr 13000) from *Desulfovibrio* species.

Concluding remarks

The aim of this study was to characterize the effect of Lys9 and Lys10 substitution in cytochrome c_7. Indeed, extensive literature data on class III multiheme cytochromes point out that the lysines surrounding the heme IV crevice modulate the heme redox potentials and provide a positive patch on the protein surface which could be important for the interaction with redox partners.

The three-dimensional solution structure of the mutated protein has been obtained by an NMR approach which combines the use of standard constraints like NOE-based upper distance limits and chemical shift constraints derived from the presence of three paramagnetic centers. An automatic assignment program was used, which allowed the quick assignment

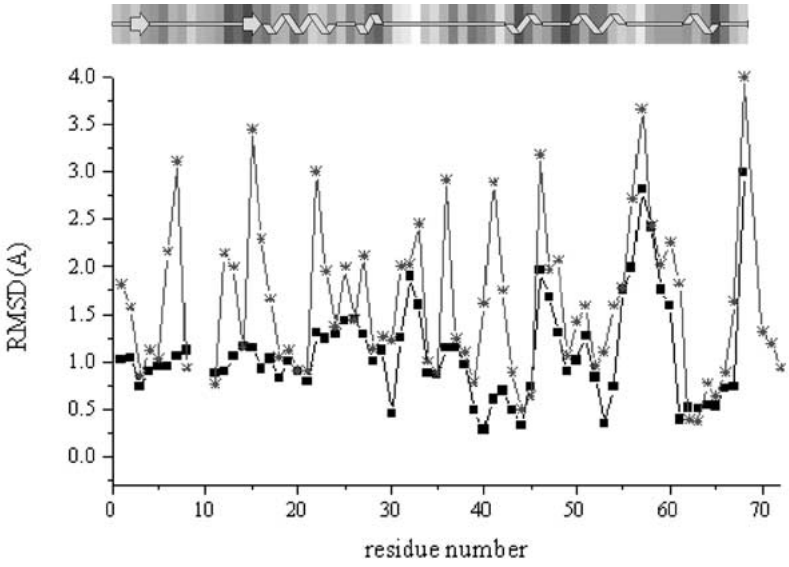

Figure 5. RMSD per residue obtained superimposing the energy minimized NMR solution structure of the K9-10A mutant with the X-ray crystal structure of the native protein. Data are reported for the backbone (■) and all heavy atoms (∗). In top, the secondary structure elements obtained with the Procheck-NMR program for the energy minimized average structure, are shown. The shading is related to the solvent accessibility of the residues, white being the most accessible and black the least. Residues 70, 71, 72 represent hemes I, III, and IV, respectively.

of proton resonances, based only on NOESY experiments.

The substitution of Lys9 and Lys10 with two alanine residues does not affect the overall fold of the protein. Nevertheless, their substitution induces subtle changes in the β-sheet formed by the two strands connected by the loop containing these amino acids and on the conformation of the His66 iron ligand of heme IV, that result close in space to the two lysines. Moreover, the removal of these two residues is probably responsible of the presence of a minor conformer detectable in the NMR spectra. The nature of this conformer has not been further analyzed here, as the shift and NOE patterns appear so similar to those of the main protein form, that it is unlikely to be able to detect real differences within the resolution of the NMR structures. Moreover, the biological significance of this conformer appears negligible, as its presence could not be inferred by measurements of redox potentials and reactivity with redox partners.

The present structure has been also carefully compared with the very recently published X-ray crystal structure of the native protein. The structures obtained with the two techniques overlay very well both in terms of backbone and prosthetic groups. Oxidized cytochrome c_7 therefore represents a nice example of the power of NMR methodology for structure determination. Although in principle the shape of this protein is quite unfavorable for a structural determination based on proton-proton dipolar interactions as required by NMR and is further complicated by the presence of three paramagnetic centers, the first solution structure was solved about 5 years before the crystal structure and the comparison of the results obtained with the two approaches show the high accuracy of the NMR-based data.

The heme iron redox potentials are essentially unaffected by the present mutations and this experimental finding is consistent with the electrostatic calculations based on the here-obtained structural information. Nevertheless, Lys10 and Lys9 appear to have a biological significance as their mutation somehow affects the reaction with the [Fe]hydrogenase. In particular a larger, although only slightly, value of K_m is found. This could be interpreted in terms of a reduced affinity of the hydrogenase towards a protein bearing a positively charge reduced by two units in an area close to the interaction region, although a possible reduction of K_m due to the presence of the minor species of the protein can not be ruled out. However, the invariance of the catalytic constants and the modest effect on K_m suggest that Lys9 and Lys10 do not represent the real interacting residues. From the structure analysis it appears that other four Lys residues are present close to heme IV but on the side of the distal His (while the mutation site is close in space to the

proximal site of hemeIV). These residues are probably those important for protein-protein recognition and electron transfer reaction, while Lys9 and 10 simply serve to enlarge the positively charged area on this protein side and reinforce the electrostatic contribution which guides the partner proteins to interact.

Acknowledgements

This work was financially supported by Italian CNR (Progetto Finalizzato Biotecnologie 99.00509.PF49) and by MURST COFIN99, and carried out under the TMR Large Scale Facility Program (EU contract No. HPRI-CT-1999-00009) and RTD FIND Structure (EU contract No. QLG2-CT-1999-01003). We gratefully acknowledge the technical assistance of Dr Gabriele Baldi with the implementation of the HANS program.

Supplementary material

The following Supplementary Material is made available:
Table S1. Assignment of the proton resonances of the fully oxidized K9-10A cytochrome c_7 at 298 K (P_i 0.1. M, pH 6.5).
Table S2. Experimental NOESY cross-peak intensities and corresponding calculated upper distance limits.
Table S3. Pseudocontact shift values.

References

Ambler, R.P. (1991) *Biochim. Biophys. Acta*, **1058**, 42–47.
Ansaldi, M., Lepelletier, M. and Mejean, V. (1996) *Anal. Biochem.*, **234**, 110–111.
Assfalg, M., Banci, L., Bertini, I., Bruschi, M., Giudici-Orticoni, M.T. and Turano, P. (1999) *Eur. J. Biochem.*, **266**, 634–643.
Assfalg, M., Banci, L., Bertini, I., Bruschi, M. and Turano, P. (1998) *Eur. J. Biochem.*, **256**, 261–270.
Aubert, C., Giudici-Orticoni, M.T., Czjzek, M., Haser, R., Bruschi, M. and Dolla, A. (1998) *Biochemistry*, **37**, 2120–2130.
Aubert, C., Lojou, E., Bianco, P., Rousset, M., Durano, M.C., Bruschi, M. and Dolla, A. (1998) *Appl. Environ. Microbiol.*, **64**, 1308–1312.
Banci, L., Bertini, I., Bren, K.L., Cremonini, M.A., Gray, H.B., Luchinat, C. and Turano, P. (1996) *J. Biol. Inorg. Chem.*, **1**, 117–126.
Banci, L., Bertini, I., Bren, K.L., Gray, H.B., Sompornpisut, P. and Turano, P. (1995) *Biochemistry*, **34**, 11385–11398.
Banci, L., Bertini, I., Bren, K.L., Gray, H.B., Sompornpisut, P. and Turano, P. (1997) *Biochemistry*, **36**, 8992–9001.
Banci, L., Bertini, I., Bruschi, M., Sompornpisut, P. and Turano, P. (1996) *Proc. Natl. Acad. Sci. USA*, **93**, 14396–14400.
Banci, L., Bertini, I., Cremonini, M.A., Gori Savellini, G., Luchinat, C., Wüthrich, K. and Güntert, P. (1998) *J. Biomol. NMR*, **12**, 553–557.
Banci, L., Bertini, I., Gori Savellini, G., Romagnoli, A., Turano, P., Cremonini, M.A., Luchinat, C. and Gray, H.B. (1997) *Proteins Struct. Funct. Genet.*, **29**, 68–76.
Bartels, C., Xia, T.H., Billeter, M., Güntert, P. and Wüthrich, K. (1995) *J. Biomol. NMR*, **5**, 1–10.
Bertini, I. and Luchinat, C. (1986) *NMR of Paramagnetic Molecules in Biological Systems*, Benjamin/Cummings, Menlo Park, CA.
Bertini, I. and Luchinat, C. (1996) *NMR of Paramagnetic Substances*, 1st edn., Coord. Chem. Rev. 150, Elsevier, Amsterdam.
Borgias, B., Thomas, P.D. and James, T.L. (1989) COmplete Relaxation Matrix Analysis (CORMA), University of California, San Francisco.
Brugna, M., Nitschke, W., Toi, H., Bruschi, M. and Giudici-Orticoni, M.T. (1999) *J. Bacteriol.*, **181**, 5505–5508.
Cambillau, C., Frey, M., Mosse, J., Guerlesquin, F. and Bruschi, M. (1988) *Proteins Struct. Funct. Genet.*, **4**, 70
Case, D.A., Pearlman, D.A., Caldwell, J.W., Cheatham, T.E., Ross, W.S., Simmerling, C.L., Darden, T.A., Merz, K.M., Stanton, R.V., Cheng, A.L., Vincent, J.J., Crowley, M., Tsui, V., Radmer, R.J., Duan, Y., Pitera, J., Massova, I., Seibel, G.L., Singh, U.C., Weiner, P.K. and Kollman, P.A. (1999) *AMBER 6*, University of California, San Francisco.
Coutinho, I., Turner, D.L., Liu, M.-Y., LeGall, J. and Xavier, A.V. (1996) *J. Biol. Inorg. Chem.*, **1**, 305–311.
Czjzek, M., Arnoux, P., Haser, R. and Shepard, W. (2001) *Acta Cryst.*, **D57**, 670–678.
Dolla, A., Leroy, G., Guerlesquin, F. and Bruschi, M. (1991) *Biochim. Biophys. Acta*, **1058**, 171–177.
Gilson, M.K., Rashin, A., Fine, R. and Honig, B. (1985) *J. Mol. Biol.*, **183**, 503–516.
Gunner, M.R. and Honig, B. (1991) *Proc. Natl. Acad. Sci. USA*, **88**, 9151–9155.
Güntert, P., Braun, W. and Wüthrich, K. (1991) *J. Mol. Biol.*, **217**, 517–530.
Güntert, P., Mumenthaler, C. and Wüthrich, K. (1997) *J. Mol. Biol.*, **273**, 283–298.
Haladjian, J., Bianco, P., Nunzi, F. and Bruschi, M. (1994) *Anal. Chem.*, **289**, 15–20.
Klapper, I., Hagstrom, R., Fine, R., Sharp, K. and Honig, B. (1986) *Proteins Struct. Funct. Genet.*, **1**, 47–59.
Koradi, R., Billeter, M. and Wüthrich, K. (1996) *J. Mol. Graphics*, **14**, 51–55.
Laskowski, R.A., MacArthur, M.W., Moss, D.S. and Thornton, J.M. (1993) *J. Appl. Crystallogr.*, **26**, 283–291.
Laskowski, R.A., Rullmann, J.A.C., MacArthur, M.W., Kaptein, R. and Thornton, J.M. (1996) *J. Biomol. NMR*, **8**, 477–486.
Macura, S., Wüthrich, K. and Ernst, R.R. (1982) *J. Magn. Reson.*, **47**, 351–357.
Marion, D. and Wüthrich, K. (1983) *Biochem. Biophys. Res. Commun.*, **113**, 967–974.
Matias, P.M., Morais, J., Coelho, R., Carrondo, M.A., Wilson, K., Dauter, Z. and Sieker, L. (1996) *Protein Sci.*, **5**, 1342–1354.
Morais, J., Palma, P.N., Frazao, C., Caldeira, J., LeGall, J., Moura, I., Moura, J.J.G. and Carrondo, M.A. (1995) *Biochemistry*, **34**, 12830–12841.
Moura, J.J.G., Moore, G.R., Williams, R.J.P., Probst, I., LeGall, J. and Xavier, A.V. (1984) *Eur. J. Biochem.*, **144**, 433–440.
Pearlman, D.A. and Case, D.A. (1991) SANDER, University of California, San Francisco.

Piotto, M., Saudek, V. and Sklenar, V. (1992) *J. Biomol. NMR*, **2**, 661–666.

Postgate, J.R. (1984) *The Sulphate Reducing Bacteria*, 2nd edn, Cambridge University Press, Cambridge.

Probst, I., Bruschi, M., Pfennig, N. and LeGall, J. (1977) *Biochim. Biophys. Acta*, **460**, 58–64.

Rousset, M., Casalot, L., Rapp-Giles, B.J., Dermoun, Z., de Philip, P., Belaich, J.P. and Wall, J.D. (1998) *Plasmid*, **39**, 114–122.

Sambrook, J., Fritsch, E.F. and Maniatis, T. (1989) *Molecular Cloning: A Laboratory Manual*. Cold Spring Harbor Laboratory Press, Cold Spring Harbor, NY.

Turner, D.L., Costa, H.S., Coutinho, I., LeGall, J. and Xavier, A.V. (1997) *Eur. J. Biochem.*, **243**, 474–481.

Weimar, P.J., van Kavelaar, M.J., Michel, C.B. and Ng, K.T. (1988) *Appl. Environ. Microbiol.*, **54**, 386–396.